Nanoscale Research Letters
a SpringerOpen Journal

NANO REVIEW   **Open Access**

Magneto-optical properties in IV-VI lead-salt semimagnetic nanocrystals

Silvio J Prado[1], Leonardo Villegas-Lelovsky[2*], Augusto M Alcalde[2], Victor Lopez-Richard[3] and Gilmar E Marques[3]

Abstract

We present a systematic study of lead-salt nanocrystals (NCs) doped with Mn. We have developed a theoretical simulation of electronic and magneto-optical properties by using a multi-band calculation including intrinsic anisotropies and magnetic field effects in the diluted magnetic semiconductor regime. Theoretical findings regarding both broken symmetry and critical phenomena were studied by contrasting two different host materials (PbSe and PbTe) and changing the confinement geometry, dot size, and magnetic doping concentration. We also pointed out the relevance of optical absorption spectra modulated by the magnetic field that characterizes these NCs.

Keywords: Nanocrystals, Quantum dots, DMS, II-VI semiconductors, Lead salts, Magneto-optical properties

Review

Recently, the successful fabrication of IV-VI nanocrystals doped with Mn has shown possible effective tuning of the emission energy from infrared (dot radius $\simeq 200$ Å) up to near-ultraviolet (dot radius $\simeq 20$ Å) regions [1]. The IV-VI semiconductors, such as PbSe nanocrystals (NCs), provide access to the limit of strong quantum confinement where, besides the changes induced by very small dot size, the direct narrow band-gap that can also be engineered by the gradual addition of dilute amounts of magnetic Mn ions to the dot structure. The members of the lead-salt family, such as PbSe and PbTe, have rock-salt crystalline structure with a direct bandgap in the L-point and the energy branches are four-fold degenerate. The bottom of the conduction band has L_6^- symmetry with the top of the valence band displaying L_6^+ symmetry of the double group D_3. This corresponds to the opposite situation observed in III-V or II-VI zinc blend materials, since here the valence band-edge Bloch function displays s-like symmetry whereas the conduction band-edge Bloch function has p_z-like symmetries, where z denotes the $\langle 111 \rangle$ direction of the cubic lattice [2].

In this letter, we contrast quantum dot electronic properties of two IV-VI semiconductor materials by modifying the quantum confinement from spherical to semispherical and varying the diluted concentration of incorporated Mn^{2+} ions. The electronic, magnetic, and optical properties are studied as a function of Mn content for varying temperature. The total Hamiltonian of the system is $H = H_{kp} + V + H_x$ where H_{kp} is the hyperbolic or Kane-Dimmock [3] $\mathbf{k} \cdot \mathbf{p}$ Hamiltonian model for IV-VI semiconductors, V is a hard wall confinement potential and H_x is the exchange interaction between Mn^{2+} ions and conduction band (valence band) spins. Here, H_{kp} was slightly modified to explore spherical symmetries of the confinements

$$
H_{kp} = \begin{bmatrix} E_g - \mathcal{D}_1^- & \frac{\hbar P_l}{m_0} P_z & 0 & \frac{\hbar P_t}{m_0} P_- \\ \frac{\hbar P_l}{m_0} P_z & \mathcal{D}_2^+ & \frac{\hbar P_t}{m_0} P_- & 0 \\ 0 & \frac{\hbar P_t}{m_0} P_+ & E_g - \mathcal{D}_1^- & \frac{\hbar P_l}{m_0} P_z \\ \frac{\hbar P_t}{m_0} P_+ & 0 & \frac{\hbar P_l}{m_0} P_z & \mathcal{D}_2^+ \end{bmatrix} \quad (1)
$$

where $\mathcal{D}_i^{\pm} = -\frac{\hbar^2 \nabla^2}{2m_t^{\pm}} + C_i P_z^2$, with ∇^2 as the 3D Laplacian operator, and $C_1 = \frac{\hbar^2}{2} \left(\frac{1}{m_l^-} - \frac{1}{m_t^-} \right)$, $C_2 = \frac{\hbar^2}{2} \left(\frac{1}{m_l^+} - \frac{1}{m_t^+} \right)$ are electron and hole effective mass terms while P_t and P_l are the anisotropic conduction-valence Kane-Dimmock coupling parameters for longitudinal and

*Correspondence: lvl@df.ufscar.br
[2]Instituto de Fisica, Universidade Federal de Uberlandia, Uberlandia, Minas Gerais 38.400-902, Brasil
Full list of author information is available at the end of the article

Springer

transverse directions; P_z and $P_\pm = P_x \pm iP_y$ are the momentum operators, whereas E_g is the bandgap and m_0 is the free electron mass. The relevant Kane-Dimmock parameters for the materials analyzed in this work can be found in [4,5].

Also, $H_x = -x/2 \langle S_z(B,T) \rangle N_0 \cdot \alpha(\cdot\beta)$, where $\langle S_z(B,T,x) \rangle$ is the mean field magnetization at temperature T, represented as a Brillouin function in dilute doped sample containing N_0 unit cells and Mn content, x [6]. Finally, α and β are the exchange constants for the semimagnetic materials, $N_0 \cdot \alpha = -0.08$ eV and $N_0 \cdot \beta = 0.02$ eV for PbMnSe, while $N_0 \cdot \alpha = -0.45$ eV and $N_0 \cdot \beta = 0.29$ eV for PbMnTe [5].

A complete set of eigenfunctions for the total Hamiltonian H can be spanned in terms of products of periodic Bloch functions $|J, J_z\rangle$ near the L-point and envelope functions. For spherical confinement, we expand the four-component spinor wave functions in two Hilbert subspaces with the general form [7,8].

$$\left| \psi_{I[II]}^M(\mathbf{r}) \right\rangle = \sum_n \sum_{L \geq |M|}^\infty \begin{pmatrix} C_{n,2L[2L+1]}^M f_{n,2L[2L+1]}^M \left| L_6^- \uparrow \right\rangle \\ C_{n,2L+1[2L]}^M f_{n,2L+1[2L]}^M \left| L_6^+ \uparrow \right\rangle \\ C_{n,2L[2L+1]}^{M+1} f_{n,2L[2L+1]}^{M+1} \left| L_6^- \downarrow \right\rangle \\ C_{n,2L+1[2L]}^{M+1} f_{n,2L+1[2L]}^{M+1} \left| L_6^+ \downarrow \right\rangle \end{pmatrix},$$

(2)

For the spherical model, these states fulfill the boundary condition $\Psi_{I,II}^M(R) = 0$ at the dot radius; thus, the function components have the form $f_{n,L}^M(r,\theta,\phi) = A_{n,L} j_L(k_n^L r) Y_L^M(\theta,\phi)$ where $A_{n,L}$ is a normalization constant, $j_L(x)$ is the spherical Bessel function, and $Y_L^M(\theta,\phi)$
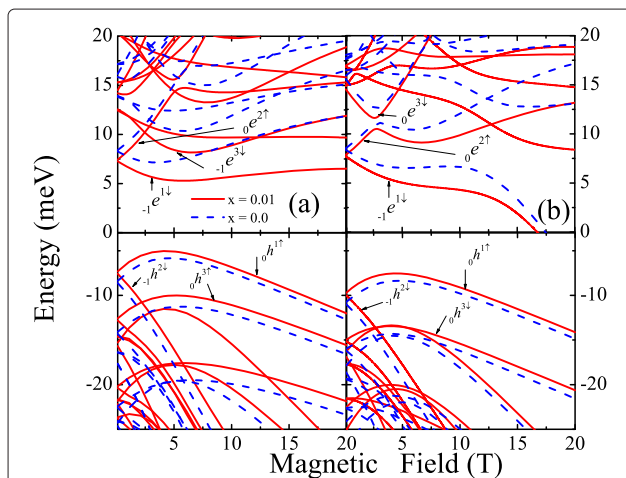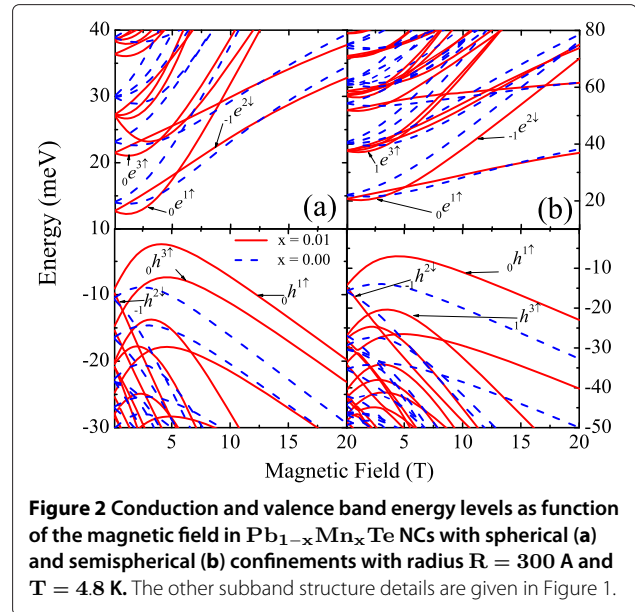

Figure 1 Conduction and valence band energy levels as function of magnetic field in $\mathbf{Pb_{1-x}Mn_x Se}$ NCs with spherical (a) and semispherical (b) confinements of radius $\mathbf{R = 300}$ A and $\mathbf{T = 1.8}$ K. The subbands structure with (solid line) and without Mn-doping (dashed line) were calculated using $E^{c(v)} - Eg(x)$.

Figure 2 Conduction and valence band energy levels as function of the magnetic field in $\mathbf{Pb_{1-x}Mn_x Te}$ NCs with spherical (a) and semispherical (b) confinements with radius $\mathbf{R = 300}$ A and $\mathbf{T = 4.8}$ K. The other subband structure details are given in Figure 1.

are the spherical harmonics. The subspaces must be constructed with special combinations of even $(f_{n,2L}^M(r))$ or odd $(f_{n,2L+1}^M(r))$ with wave number $k_n^L = \mu_n^l/R$, where μ_n^l is the nth zero of $j_L(x) = 0$. For the semispherical structures, the states must also fulfill the boundary condition $\Psi_{I,II}^M(r, \theta = \frac{\pi}{2}, \phi) = 0$ at the equator plane which restricts the set of quantum numbers L and M to the condition $|L - M| = $ odd number. Hence, the parities of the spinor components differ from the full spherical case and the states $\left| \psi_{I[II]}^M(\mathbf{r}) \right\rangle$ for a semispherical confinement require the replacement $2L (2L + 1)$ in the second (third) line of Equation 2 by $2L + 1 (2L)$.

Figure 1a,b shows the changes in the magnetic energy dispersions for the first few levels in $Pb_{1-x}Mn_xSe$ dots with $R = 300$ A when the confinement is changed from spherical to semispherical. The broken symmetry induces stronger changes on the electron than on the hole energy dispersions by inducing anti-crossing regions. The exchange coupling affects mainly the conduction carrier dispersion. However, for $Pb_{1-x}Mn_xTe$ dots with the same size R, shown in Figure 2a,b with both broken symmetry and exchange interaction, induce strong changes on both carrier magnetic dispersions but with the valence-band being more sensitive. The interplay between the usual Zeeman effect and the exchange interaction gives place to the crossing between spin-split levels at certain critical field, B_c, as displayed in Figure 2 for both spherical and semispherical dot spatial confinements.

Figure 3a,b shows that the critical field strength for $Pb_{1-x}Mn_xTe$ dots, at a fixed temperature, increases with increasing Mn content for different dot sizes. Note that the smaller the dot size R, the larger the critical
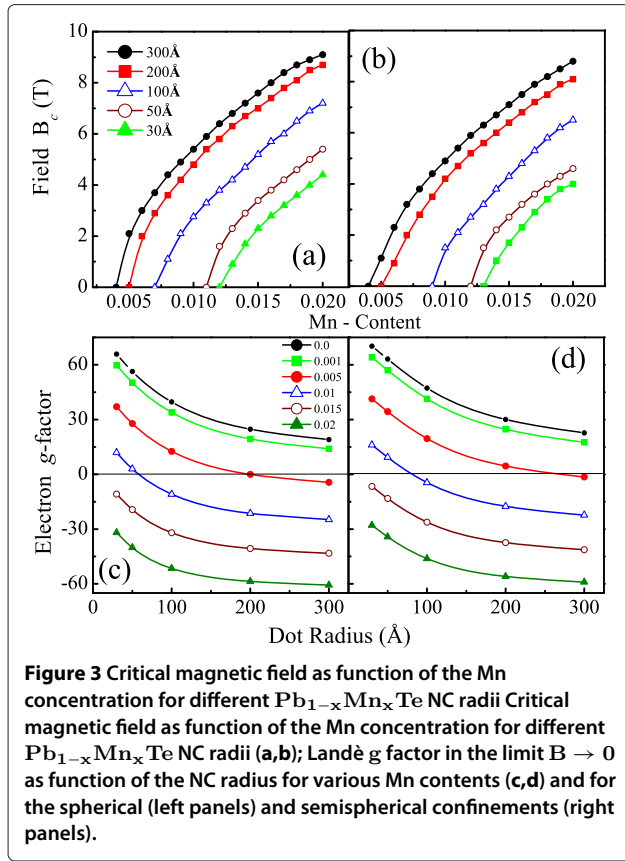
Figure 3 Critical magnetic field as function of the Mn concentration for different $\mathbf{Pb_{1-x}Mn_xTe}$ NC radii Critical magnetic field as function of the Mn concentration for different $\mathbf{Pb_{1-x}Mn_xTe}$ NC radii (**a,b**); Landè g factor in the limit $B \to 0$ as function of the NC radius for various Mn contents (**c,d**) and for the spherical (left panels) and semispherical confinements (right panels).

concentration x_c where $B_c \Rightarrow 0$. For the limit $B \to 0$, we have calculated the Landè g-factor of the conduction band ground state of $Pb_{1-x}Mn_xTe$ dots as $g_e \mu_B B = E(e \uparrow, 1/2, N) - E(e \downarrow, -1/2, N)$, where $\mu_B = e\hbar/(2m_0 c)$ is the Bohr magneton, $E(e \uparrow (\downarrow), F_z, N)$ is the energy of the corresponding spin state, and $F_z = L_z + J_z$ is the z-component of total angular momentum $\mathbf{F} = \mathbf{L} + \mathbf{S}$. The g_e-values for $Pb_{1-x}Mn_xTe$ dots as shown in Figure 3c,d displays similar behavior as reported in [9,10] $g_e(B, R, x)$ to approximately $1/R$.

As noted in Figure 3c,d, there are Mn concentration regions where the g factor becomes strictly positive or negative, independent of the confinement shape. For fixed dot radius, it is possible to predict the existence of a zero critical field value for a certain value x_c for different dot and confinement geometries. For large dot sizes, a nonlinear increasing of B_c is observed for low values of x and a quasi-linear behavior otherwise.

In order to discuss the optical absorption spectrum, the probability for dipole-allowed optical transitions between single electron and hole states has to be evaluated in detail. Within the electrical dipole approximation, the oscillator strength is a linear combination of the matrix elements of the optical transitions, $M_{j,j'} = \langle \psi_j | \widehat{\mathbf{e}}.\widehat{\mathbf{P}} | \psi_{j'} \rangle = \langle f_j | f_{j'} \rangle . \langle u_j | \widehat{\mathbf{e}}.\widehat{\mathbf{P}} | u_{j'} \rangle + \langle u_j | u_{j'} \rangle . \langle f_j | \widehat{\mathbf{e}}.\widehat{\mathbf{P}} | f_{j'} \rangle$. Here, $\widehat{\mathbf{e}}$ is the light

polarization vector, $\widehat{\mathbf{P}}$ is the momentum operator, f_j and u_j are the envelope and periodic Bloch functions at the L point for each involved carrier j, respectively. The second term on the right-hand side is responsible for intraband optical transitions, since $\langle u_j | u_{j'} \rangle = \delta_{jj'}$. In this case the incident light couples, in the same band, state with different symmetries whenever the term $\langle f_j | \widehat{\mathbf{e}}.\widehat{\mathbf{P}} | f_{j'} \rangle \neq 0$ for a given polarization. In our case the complete set of selection rules are obtained from the nonvanishing products of the matrix elements $I_{e,h} \delta_{L_e, L_h} \Pi_{\alpha, \alpha'}$, where $\Pi_{\alpha, \alpha'}$ is the matrix of the parity operator, and $I_{e,h} = \langle f_{e,\alpha} | f_{h,\alpha} \rangle$ is the overlap integral of the electron-hole envelope functions allowed by the interband transition $\alpha \to \alpha'$. The allowed transitions between states belonging to the Hilbert subspaces described by spinors (2) are determined from the angular dependence of the wave functions $f_{n,L}^M(r)$.

The corresponding selection rules for each optical transition in any polarization can be precisely obtained according to Kang et al.[2]. Due to the differences in the angular momenta L (symmetry and parity) of electron and hole spinor components, the allowed transitions occur only between initial (hole) and final (electron) states belonging to different Hilbert subspaces ($I \Rightarrow II$ or $II \Rightarrow I$) for linear light polarization π^z and for circular light polarization $\sigma^{\pm}$. Moreover, the preservation of the total angular momentum F_z, between initial and final states requires that $\Delta M = 0$ for Voigt- π^z, and $\Delta M = \pm 1$ for Faraday- $\sigma^{\pm}$ geometry. For the circular polarization, the optical matrix element takes the form

$$\langle \psi_{e,I}^{M_e} | \widehat{\mathbf{e}}^{\pm} \cdot \widehat{\mathbf{P}} | \psi_{h,II}^{M_h} \rangle = P \mathcal{F}_{N_e, M_e}^{N_h, M_h}(I, II) \delta_{M_e, M_h \pm 1}, \quad (3)$$

where

$$\mathcal{F}_{N_e, M_e}^{N_h, M_h}(I, II) = \sum_{n, L \geq |M|} \left[C_{n,\beta}^{e\pm} C_{n,\beta}^{e\pm} + C_{n,\beta}^{h\pm} C_{n,\beta}^{h\pm} \right], \quad (4)$$

with $\beta = 2L + 1/2 \mp 1/2$. In the same way, the $I \to II$ transitions can be obtained by interchanging $2L + 1/2 \mp 1/2$ by $2L + 1/2 \pm 1/2$. The absorption coefficient can then be written as follows [7]:

$$\alpha(\widehat{\mathbf{e}}^{\pm}, \omega) = \alpha_0 \sum_{N_e, N_h, M} \left(\frac{\Gamma}{\pi} \right)$$
$$\times \left(\frac{\left| \mathcal{F}_{N_e, M}^{N_h, M \pm 1}(I, II) \right|^2}{[E_{N_e, M}(I) - E_{N_h, M \pm 1}(II) - \hbar\omega]^2 + \Gamma^2} \right.$$
$$\left. + \frac{\left| \mathcal{F}_{N_e, M}^{N_h, M \mp 1}(I, II) \right|^2}{[E_{N_e, M}(II) - E_{N_h, M \mp 1}(I) - \hbar\omega]^2 + \Gamma^2} \right), \quad (5)$$
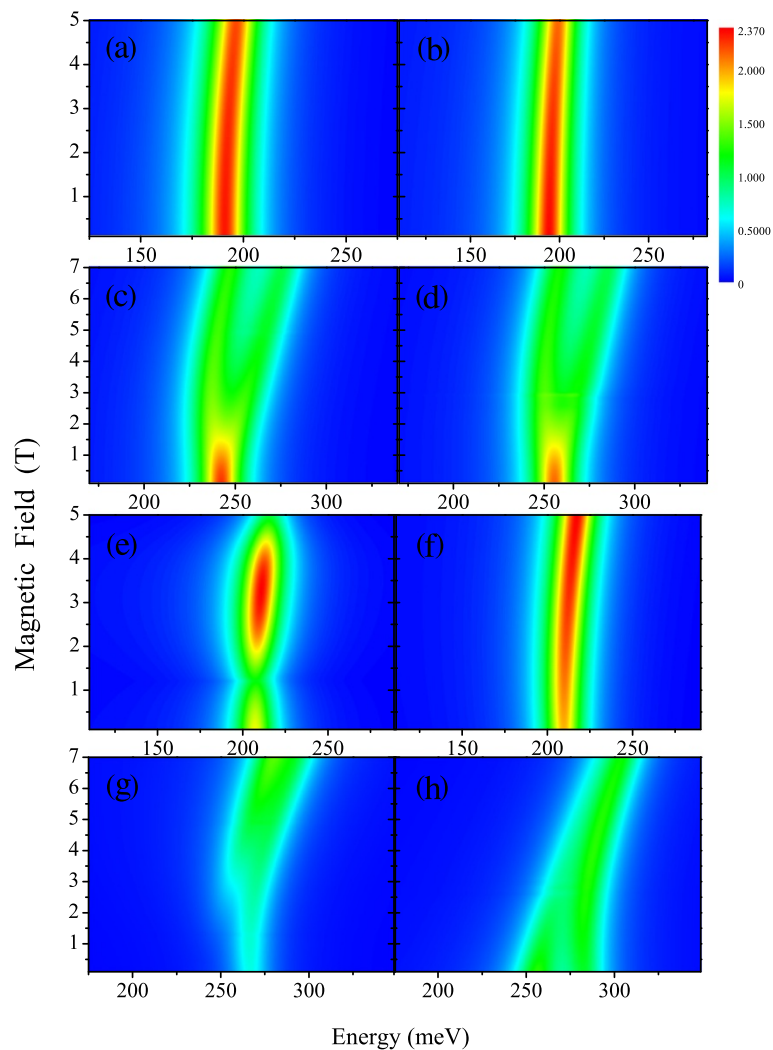
Figure 4 Interband absorption spectra as function of magnetic field for polarization π^z (a-d) and σ^+ (e-h) $\mathrm{Pb_{0.99}Mn_{0.01}Se}$ NCs with spherical (a,e) and semispherical (b,f) confinements and $\mathrm{Pb_{0.99}Mn_{0.01}Te}$ NC with spherical (c,g) and semispherical (d,h) confinements. The same parameters were as referred in Figures 1 and 2.

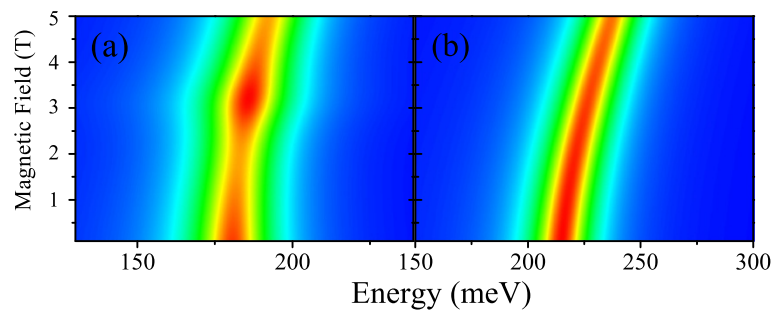**Figure 5 Interband absorption spectra as function of magnetic field for polarization σ^+ of PbSe (a) and PbTe NCs (b) with spherical confinement of $\mathrm{R} = 300$ A and temperatures 1.8 and 4.8 K, respectively.**

where α_0 is a magnitude which includes the bulk P parameter and the dielectric constant. The material parameters can be found in [4,5]. For the linear light polarization π^z, the optical matrix element becomes

$$\left\langle \psi_{e,I}^{M_e} | \hat{\mathbf{e}}^{\pm} \cdot \widehat{\mathbf{P}} | \psi_{h,II}^{M_h} \right\rangle = P \mathcal{V}_{N_e,M_e}^{N_h,M_h}(I,II) \delta_{M_e,M_h \pm 1}, \qquad (6)$$

where

$$\mathcal{V}_{N_e,M_e}^{N_h,M_h}(I,II) = \sum_{n,L \geq |M|} \left[C_{n,\beta}^{e^+} C_{n,\beta}^{h^+} + C_{n,\beta}^{e^-} C_{n,\beta}^{h^-} \right], \qquad (7)$$

and the related absorption coefficient turns

$$\alpha(\hat{\mathbf{e}}^z,\omega) = \alpha_0 \sum_{N_e,N_h,M} \left(\frac{\Gamma}{\pi} \right)$$

$$\times \left(\frac{\left| \mathcal{V}_{N_e,M}^{N_h,M}(I,II) \right|^2}{[E_{N_e,M}(I) - E_{N_h,M}(II) - \hbar\omega]^2 + \Gamma^2} \right.$$

$$\left. + \frac{\left| \mathcal{V}_{N_e,M}^{N_h,M}(I,II) \right|^2}{[E_{N_e,M}(II) - E_{N_h,M}(I) - \hbar\omega]^2 + \Gamma^2} \right). \quad (8)$$

In the case of semispherical geometry, the selection rules for the circular light polarization are the same as for the spherical case; meanwhile, for the linear light polarization, these allow transitions within the same subspace due to the parities of the components of the wave functions in the subspaces.

The excitonic resonances for π^z and σ^+, calculated as a function of the magnetic field for each Mn-doped lead-salt dot and confinements, are shown in Figure 4a,b,c,d,e,f,g,h. In Figure 5, we displayed the corresponding excitonic resonances for σ^+ of the reference samples (without Mn doping) for spherical confinement. Comparing Figures 4e and 5a and Figures 4g and 5b, we confirm that the effect of Mn doping on the absorption spectra is stronger on the bandgap renormalization than on the subband levels in the doped salt-selenide unlike the salt-telluride, where the Mn presence strongly modifies all the band structure [11,12]. The resonant transitions shown in Figure 5a,b involve just the conduction band ground state of spherical and semispherical PbMnSe dots. The corresponding spectra for PbMnTe, shown in Figure 4c,d, correspond to the transitions to the first crossing conduction band levels. Figure 4d displays an absorption bottleneck due to the level crossing (see Figure 2a,b) for PbMnSe spherical dots. Another absorption quenching appears at $B = 1.2$T in Figure 4e caused by the character admixture close to a level crossing. In turn, Figure 4f displays a single transition to the conduction band ground state. In Figures 4g,h two transitions appear that fade-off for lower and higher fields, respectively. This effect is produced by the modulation

of the oscillator strength. For small nanocrystal size, the spectra will show quantitative variation due to the effective gap modulation and the subsequent weakening of the intersubband coupling.

Conclusions

Summarizing, we have investigated the electronic and magneto-optical properties of $Pb_{1-x}Mn_xSe$ and $Pb_{1-x}Mn_xTe$ semimagnetic dots by taking advantage of their strong sensitivity to spatial confinement asymmetry and properties induced by the Mn doping. We have shown the appearance of the critical phenomena as the spin level crossing for certain concentration of Mn on the $Pb_{1-x}Mn_xTe$ and the modulation of the optical absorption controlled by field B and confinement anisotropy. Subtle effects of Mn content variation were predicted for the energy spectra of the $Pb_{1-x}Mn_xSe$ dots, whereas important consequences are expected for $Pb_{1-x}Mn_xTe$ dots. We believe that these results may stimulate research groups working on these important materials to explore device applications working on the wide spectral range.

Author details
[1]Faculdade de Ciencias Integradas do Pontal, Universidade Federal de Uberlandia, Ituiutaba Minas Gerais 38302-000, Brasil. [2]Instituto de Fisica, Universidade Federal de Uberlandia, Uberlandia, Minas Gerais 38.400-902, Brasil. [3]Departamento de Fisica, Universidade Federal de Sao Carlos, Sao Carlos, Sao Paulo 13.565-905, Brasil.

Authors' contributions
SJP carried out the calculation of the band structure and absorption spectra and participated in the study of the electronic and magneto-optical properties. LVL, VLR and GEM participated in the design of the problem, and its study and coordination. AMA conceived of the study and participated in the design of the problem and first stages of calculation. All authors read and approved the final manuscript.

References
1. Dantas NO, Silva RS, Pelegrini F, Marques GE: **Morphology in semimagnetic** $Pb_{1-x}Mn_xSe$ **nanocrystals: thermal annealing effects.** *Appl Phys Lett* 2009, **94**:263103.
2. Kang I, Wise FW: **Electronic structure and optical properties of PbS and PbSe quantum dots.** *J Opt Soc Am B* 1997, **14**:1632.
3. Dimmock JO: *Physics of Semimetals and Narrow Gap Semiconductors*(Carter DL, Bate RT, eds.) Oxford: Pergamon; 1971.
4. Pascher H, Bauer G, Grisar R: **Magnetooptical investigations and four-wave-mixing spectroscopy of PbSe.** *Phys Rev B* 1988, **38**:3383.
5. Hota RL, Tripathi GS, Mohanty JN: **Theory of effective g factors and effective masses in diluted magnetic semiconductors.** *Phys Rev B* 1993, **47**:9319.
6. Marques GE: *Diluted Magnetic Semiconductors*. 1st edition(Jain M, ed.) Singapore: World Scientific; 1990.

7.   Prado SJ, Trallero-Giner C, Alcalde AM, López-Richard V, Marques GE:
     Magneto-optical properties of nanocrystals: Zeeman splitting. *Phys Rev B* 2003, **67:**165306.
8.   Prado SJ, Trallero-Giner C, Alcalde AM, López-Richard V, Marques GE:
     Optical transitions in a single CdTe spherical quantum dot. *Phys Rev B* 2003, **68:**235327.
9.   Prado SJ, Trallero-Giner C, Alcalde AM, López-Richard V, Marques GE:
     Influence of quantum dot shape on the Landé g-factor determination. *Phys Rev B* 2004, **69:**201310 (R).
10. López-Richard V, Prado SJ, Marques GE, Trallero-Giner C, Alcalde AM:
     Manipulation of g-factor in diluted magnetic semiconductors quantum dots: optical switching control. *Appl Phys Lett* 2006, **88:**052101.
11. Lusakowski A, Dugaev VK: **Ground state splitting for the Mn^{2+} ion in PbMnTe compounds.** *Phys Rev B* 2005, **71:**014422.
12. Lusakowski A, Boguslawski P, Radzyński T: **Calculated electronic structure of $Pb_{1-x}Mn_xTe$ ($0 \leq x < 11\%$): the role of L and Σ valence band maxima.** *Phys Rev B* 2011, **83:**115206.